An Undular Bore and Gravity Waves Illustrated by Dramatic Time-Lapse Photography

TIMOTHY A. COLEMAN AND KEVIN R. KNUPP

Department of Atmospheric Science, University of Alabama in Huntsville, Huntsville, Alabama

DARYL E. HERZMANN

Department of Agronomy, Iowa State University, Ames, Iowa

(Manuscript received 24 March 2010, in final form 17 May 2010)

ABSTRACT

On 6 May 2007, an intense atmospheric undular bore moved over eastern Iowa. A ''Webcam'' in Tama, Iowa, captured dramatic images of the effects of the bore and associated gravity waves on cloud features, because its viewing angle was almost normal to the propagation direction of the waves. The time lapse of these images has become a well-known illustration of atmospheric gravity waves. The environment was favorable for bore formation, with a wave-reflecting unstable layer above a low-level stable layer. Surface pressure and wind data are correlated for the waves in the bore, and horizontal wind oscillations are also shown by Doppler radar data. Quantitative analysis of the time-lapse photography shows that the sky brightens in wave troughs because of subsidence and darkens in wave ridges because of ascent.

1. Introduction

During the morning hours of 6 May 2007, an intense atmospheric bore, with a pressure perturbation of 4 hPa, was generated over eastern Iowa. The bore was undular, with a train of distinctive gravity waves following its passage. A ''Webcam'' in Tama, Iowa, captured over 40 min of video showing the effects of the gravity waves on cloud features. Photographs of the cloud features associated with bores have been published previously (e.g., Clarke et al. 1981; Wakimoto and Kingsmill 1995). However, on 6 May 2007, the camera at Tama was oriented such that its direction of view was normal to the direction of wave propagation, allowing for a fairly unique visual analysis of the structure and kinematics of the bore and associated gravity waves (see Fig. 1).

An atmospheric bore is a propagating hydraulic jump, typically associated with a sudden increase in the depth of a stable boundary layer and a sudden rise in pressure, and it may form when a density current impinges on a stable layer (e.g., Christie et al. 1978; Crook 1986; Rottman and Simpson 1989; Koch et al. 2008; Hartung et al. 2010). There is typically an energy imbalance across the bore. The form of the dissipation of the energy is related to the bore strength h_1/h_0, where h_0 is the initial depth of the stable layer and h_1 is its postbore depth. When $1 < h_1/h_0 < 2$, the energy is released in the form of gravity waves behind the bore. When $2 < h_1/h_0 < 4$, the bore is still undular, but some turbulent mixing occurs. When $h_1/h_0 > 4$, the energy is released entirely in the form of turbulence (Rottman and Simpson 1989; Simpson 1997). A wave duct or wave-trapping mechanism (e.g., Lindzen and Tung 1976; Nappo 2002) may also be necessary for a bore to propagate over a significant distance (e.g., Crook 1986).

2. Data and methodology

The primary dataset is the time-lapse video captured by the Tama Webcam, located at 41.99°N, 92.65°W. The camera is jointly operated by KCCI-TV and the Iowa Environmental Mesonet (IEM) of Iowa State University. The individual frames of the video provide a still image every 2.48 s. The optical depth of sinusoidal cloud bands, shown by the normalized intensity of light (e.g., Coleman et al. 2009) near cloud base, illustrates the vertical motion associated with the gravity waves, whereas the motion of cloud fragments shows the wind and the wind perturbations may be inferred.

Corresponding author address: Tim Coleman, Department of Atmospheric Science, University of Alabama in Huntsville, NSSTC, 320 Sparkman Drive, Huntsville, AL 35805.
E-mail: coleman@nsstc.uah.edu

DOI: 10.1175/2010JTECHA1472.1

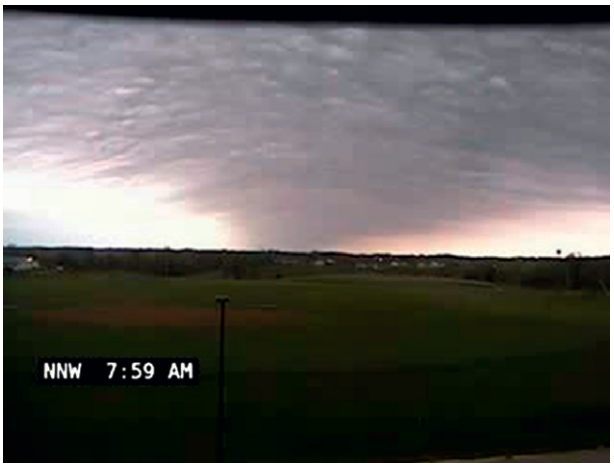

FIG. 1. The first frame in the 40-min time-lapse video from Tama, Iowa, starting at 1259 UTC. This image, looking north-northwest (perpendicular to bore motion) shows the leading edge of the undular bore (darker cloud shading associated with lift and condensation, near center) and the approach of the first postbore gravity wave trough (clouds curving downward on left and lightening because of subsidence and drying).

Surface pressure and wind data are analyzed in conjunction with Weather Surveillance Radar-1988 Doppler (WSR-88D) data to determine the kinematics of the bore and waves. Model soundings (containing 23 vertical levels between the surface and 12 km MSL) from the 1200 UTC North American Mesoscale (NAM) model, every 0.5° longitude, are used to construct east–west vertical cross sections of potential temperature θ, Brunt–Väisälä frequency N, the component of the wind in the direction of the bore u, and the Scorer parameter l^2. This allows insight into the initiation of the bore and, in conjunction with surface data, approximations of bore strength.

3. Environment, initiation, and analysis of the undular bore

During the morning hours of 6 May 2007, a mesoscale convective system (MCS) extended from central Iowa to northeast Kansas. As the MCS moved into central Iowa, it began to encounter cooler and more stable air at low levels. Figure 2 shows the east–west vertical cross sections discussed in section 2, along 42°N (near Tama's latitude) and from 96° to 90°W (roughly covering the state of Iowa at that latitude). Surface temperatures decrease about 5 K from the western edge of Iowa, where convection was more active, to Tama, where the bore was photographed. The static stability also increased significantly between 500 and 1500 m MSL in areas east of 94°W. The Brunt–Väisälä frequency N at 1 km MSL increased from near 0.012 s^{-1} in western Iowa to near 0.025 s^{-1} in central Iowa. This represents the stable layer that the MCS and its cold pool impinged on, producing the bore.

The wave-trapping mechanism necessary for the bore and gravity waves to propagate over long distances was also in place above the stable layer. A wave-reflecting layer may be caused by a decrease in the Scorer parameter l^2 (Scorer 1949) with height, where l^2 is proportional to N^2 and the curvature of the wave-parallel component of the wind profile (d^2u/dz^2; e.g., Nappo 2002). As shown in Fig. 2, on 6 May 2007 the static stability N^2 decreased with height above 1500 m MSL and a wave-parallel jet maximum was also present near 1700 m MSL. Therefore, l^2 decreased from 50×10^{-7} m^{-2} in the layer between 1000 and 2500 m MSL to near zero at 4000 m MSL near Tama (92.65°W). This provided the necessary decrease in Scorer parameter l^2 with height for wave trapping.

The pressure jump associated with the bore was first detected clearly at two stations 40–50 km southwest of Tama, between 1205 and 1215 UTC. The surface observations at Tama, the site of the Webcam (Fig. 3), are strongly indicative of an undular bore. The pressure jumped 3.4 hPa between 1247 and 1259 UTC, as the depth of the stable layer increased. Then, three distinct oscillations in pressure occurred, with periods of 12–14 min, as the gravity waves behind the bore passed by. The amplitudes of these waves were 2.1, 0.9, and 0.2 hPa, consistent with amplitude-ordered waves (e.g., Christie 1989).

The component of the wind parallel to the disturbance motion u was also consistent with an undular bore. The near-surface wind surged from $u = -15$ m s^{-1} at the leading edge of the bore to 5 m s^{-1} at the peak of the pressure jump, a change of 20 m s^{-1}. The wind oscillated as the gravity waves passed, with winds in the direction of wave motion in pressure ridges and in the opposite direction in pressure troughs, consistent with the impedance relationship stating the correlation between p' and u' that is typically observed in gravity waves (Gossard and Hooke 1975; Koch and O'Handley 1997). The surface temperature (not shown) remained constant (within the 0.55°C accuracy range of the instrument) throughout the initial pressure jump, consistent with a bore, as opposed to a density current, where the temperature would drop.

To verify the nature of the bore and its speed, the surface data at Tama were combined with 1200 UTC NAM data (see Fig. 2). According to NAM data, $h_0 =$ 950 m at Tama. Based on the 3.5-hPa pressure jump, the postbore depth of the stable layer was computed, using an iterative approach and the hydrostatic equation, to be approximately $h_1 = 1650$ m. This implies a bore strength

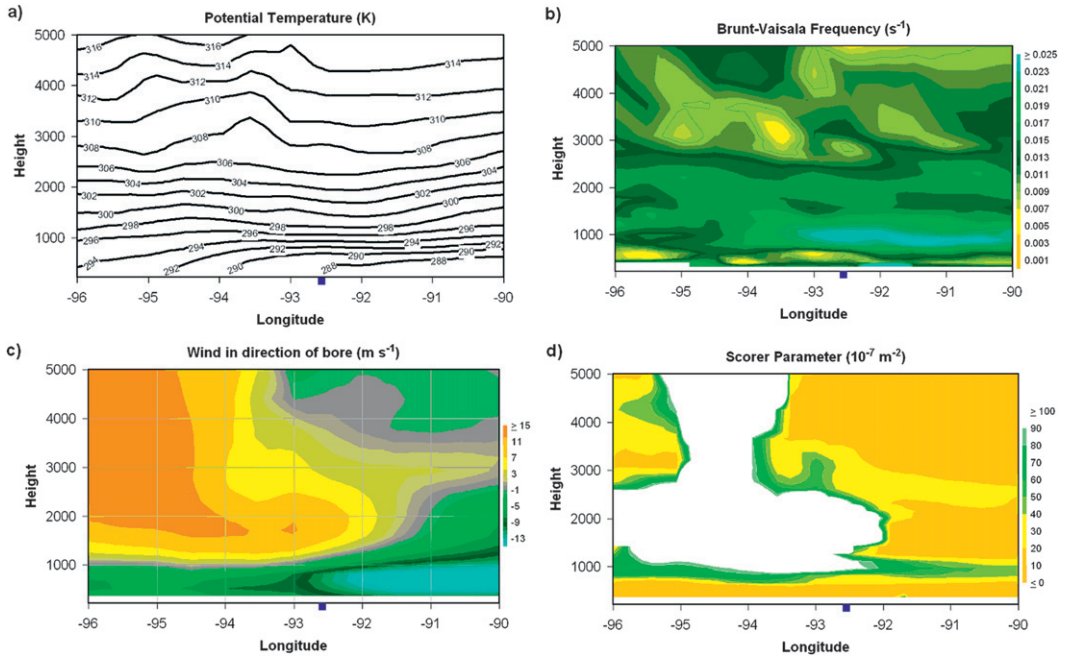

FIG. 2. East–west cross sections at 42°N of NAM model output (1200 UTC 6 May 2007) of (a) potential temperature (K), (b) Brunt–Väisälä frequency (s^{-1}), (c) the component of the ambient wind in the direction of bore propagation (m s^{-1}), and (d) the Scorer parameter (10^{-7} m^{-2}). The Tama camera was located at approximately 92.65°W (shown by the blue squares). The x axes (longitudes from −96 through −90) roughly indicate the boundaries of the state of Iowa.

$h_1/h_0 = 1.7$, indicating that the bore should be smooth and undular. Using shallow-water hydraulic theory, the intrinsic bore speed may be written as (adapted from Rottman and Simpson 1989; Knupp 2006)

$$C_{\text{bore}} = \left[g \frac{\Delta\theta_v}{\theta_v} \frac{h_1}{2} \left(1 + \frac{h_1}{h_0} \right) \right]^{1/2}, \qquad (1)$$

where θ_v is the average virtual potential temperature in the stable layer (293 ± 1 K) and $\Delta\theta_v$ is the difference between the average θ_v in the stable layer and that in the less stable layer above (300 K). This calculation shows an intrinsic bore speed of 22.8 (±1.5) m s^{-1}; because the wave-parallel component of the background wind in the stable layer was $U = -8$ m s^{-1}, the ground relative speed of the bore should theoretically be 14.8 (±1.5) m s^{-1}.

The MCS that initiated the bore is shown on radar at 1102 UTC (Fig. 4). A fine line propagating ahead of the MCS can be seen in radar reflectivity data, at least as early as 1222 UTC. This fine line represents the leading edge of the undular bore. Radar data indicate that the bore was propagating toward 80° near 11.5 m s^{-1}, somewhat smaller than the theoretical speed, but close to the range, given the estimates required to produce the theoretical speed. By 1316 UTC, gravity waves had developed behind the bore and appear clearly as bands in the radial velocity data image (Fig. 4c). A cross section of radial velocity data was constructed along 80° azimuth at 1316 UTC (Fig. 4d). The bore is indicated by the large region of outbound radial velocities near 110-km range. The oscillations in radial velocity behind the bore, at ranges from 85 to 110 km, indicate the gravity waves behind the bore and have horizontal wavelengths of 8 km. The speed implies a wave period of 11.6 min. At least two full wavelengths of waves are indicated,

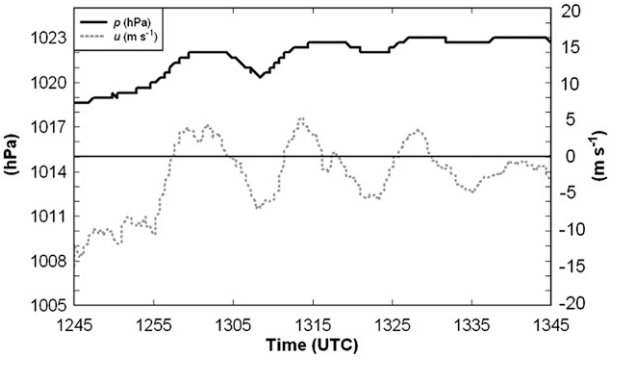

FIG. 3. Surface observations (at 12-s resolution) at the location of the Tama Webcam of MSL pressure (hPa; solid dark curve) and the 1-min average of the component of the wind in the direction of the bore and wave motion (m s^{-1}; dashed gray curve).

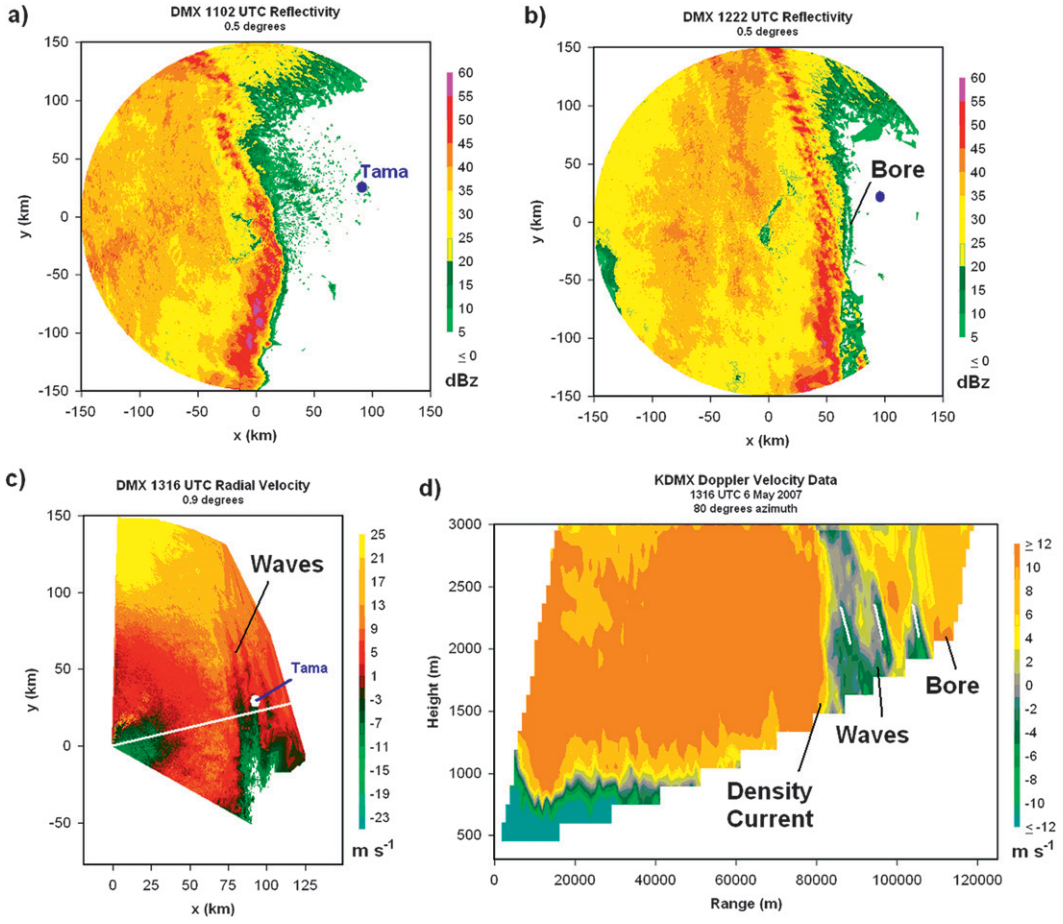

FIG. 4. Plan position indicator (PPI) images of reflectivity (dBZ) from Des Moines, Iowa, WSR-88D radar (KDMX) at 0.5° elevation at (a) 1102 and (b) 1222 UTC 6 May 2007. Bore is indicated by the fine line separating from MCS. (c) PPI image of radial velocity (m s^{-1}) at 0.9° elevation from KDMX radar at 1316 UTC. Banded velocity signature indicates locations of gravity waves. (d) Cross section of KDMX radial velocity data (m s^{-1}) at 1316 UTC, along 80° azimuth [indicated by white line in (c)]. The inbound and outbound oscillations in velocity clearly show the gravity waves and the bore. Small white lines indicate phase lines along wave troughs. The radar is located at the origin in (a)–(d). The location of the Tama Webcam is indicated in (a)–(c) and is very near a range of 100 km in (d).

consistent with surface observations of wind and pressure and, as will be shown, with time-lapse photography.

4. Analysis of time-lapse photography

Time-lapse photography, at 2.48-s resolution, is available from the Tama Webcam for the period 1259:40–1340:00 UTC [7:59 a.m. through 8:40 a.m. central daylight time (CDT)] for a total of 977 images. The entire sequence of time-lapse photographs is available as an animation and a video (at the time of writing it is available online at http://vortex.nsstc.uah.edu/~coleman/wave; the video is also available online at http://www.youtube.com/watch?v=yXnkzeCU3bE). Six individual frames are shown in Fig. 5. As stated above, the view of the camera was parallel to the linear cloud features associated with the bore and gravity waves. This sequence of photographs, perhaps more than any published, clearly illustrates the sinusoidal shape of the mesoscale cloud base caused by the gravity waves and the bore.

Strong ascent at the leading edge of the bore created significant condensation (as shown on radar in Fig. 4b), producing the band of dark clouds in Fig. 5a at 1300 UTC. This is consistent with the time of arrival of the main pressure jump associated with the bore, shown in Fig. 3a (a nearby surface observation prior to the MCS indicated cloud heights around 1400 m AGL). Subsidence ahead of the first gravity wave trough causes the cloud base to lower because of downward advection of cloud water (Fig. 5b), producing a convex appearance to the ceiling. However, the subsidence-induced warming clearly evaporates some of the cloud water in the wave

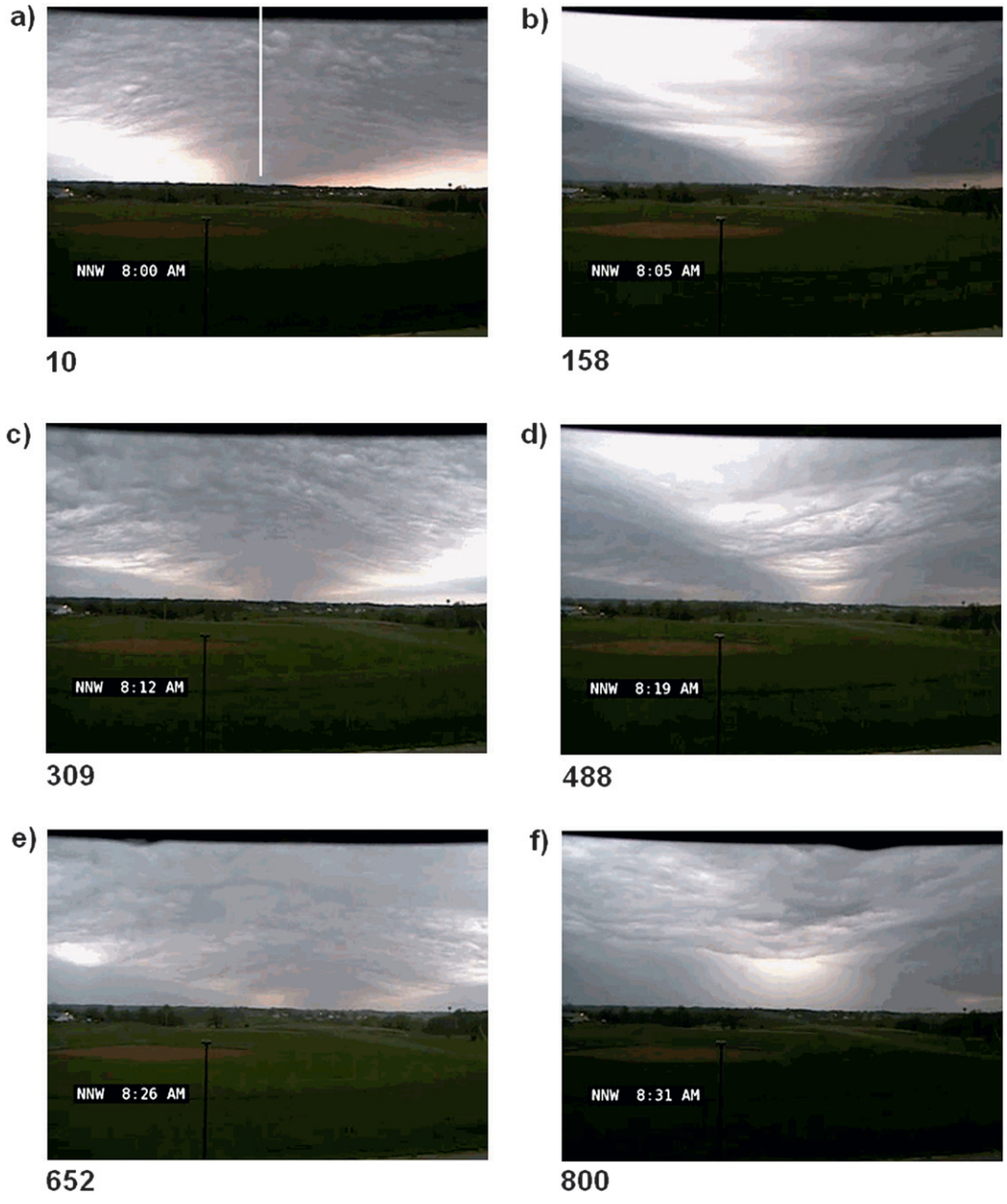

FIG. 5. Still image frames (with frame numbers to bottom left of each) extracted from time-lapse video of bore and gravity waves from Tama Webcam. The view in all six images is north-northwest, perpendicular to the motion of the bore and the associated waves. The times for the images are (a) 1300:00 (leading edge of bore), (b) 1306:12 (first gravity wave trough), (c) 1312:24 (first wave ridge), (d) 1319:51 (second wave trough), (e) 1326:37 (second wave ridge), and (f) 1332:45 UTC (third wave trough).

trough, reducing the optical depth of the cloud layer and allowing more sunlight to shine through in the wave trough around 1306 UTC. This subsidence warming is consistent with the hydrostatically produced pressure trough at the surface at 1306 UTC (Fig. 3a). As the first gravity wave ridge approaches, upward motion advects cloud water back upward and the cloud base rises, forming a concave ceiling at 1312 UTC (Fig. 5c). The rising motion produces cooling and an associated surface pressure ridge at 1312 UTC (Fig. 3a), and it produces additional condensation of cloud water, increasing the optical depth of the cloud layer, allowing less sunlight to reach the cloud

base. There may also be some slight turbulence in the wave ridges, but the troughs appear smooth and the bore is overall undular, consistent with its bore strength.

This entire process, including subsidence causing lowering, convexity, and thinning of the cloud layer (and brightening of the sky) in the troughs and ascent causing lifting, concavity, and thickening of the cloud layer (and darkening of the sky) in the ridges, occurs over another 1.5 periods of gravity waves between 1312 and 1331 UTC (Figs. 5d–f). Throughout the period from 1300 through 1331 UTC shown in Fig. 5, the behavior of the cloud base (height and shape) and the brightness of the sky associated with condensation and evaporation are consistent in time with the pressure troughs and ridges shown in Fig. 3a.

The aforementioned effects of the waves on the brightness of the sky are quantified in Fig. 6. In each digital photograph in the time lapse, a vertical section of 22 pixels at the top of each image, centered horizontally in the photograph (as shown in Fig. 5a), was processed using ''Pixel Profile'' (Glynn 2003) image analysis software. These 22-pixel sections represented the sky in the center of each image. For the 22-pixel section in each photograph, the normalized light intensity ($0 < I < 256$) was retrieved, and this light intensity is plotted versus time in Fig. 6. The sky is fairly dark ($I = 145$) at the time of passage of the leading edge of the bore. The sky becomes about 50% brighter just ahead of the first gravity wave–associated pressure trough around 1307 UTC ($I = 228$) and then becomes significantly darker again ($I = 132$) at 1311 UTC, about 3 min before the first pressure ridge. The sky brightens around 1320 UTC, only 1 min ahead of the second pressure trough, and then darkens again around 1326 UTC, as the second pressure ridge moves in. The light intensity becomes noisy after 1326 UTC, but an overall brightening of the sky can be inferred associated with the very weak third wave trough at 1333 UTC. Note that, like the pressure oscillations, the amplitudes of the changes in light intensity decrease with each wave. The period of the oscillations in light intensity is about 12 min, very close to the wave period of 11.6 min determined using radar data in section 3.

Finally, though impossible to visualize in the static images in this paper, the time-lapse video also shows the perturbation horizontal motions associated with the gravity waves in the cloud fragments. Consistent with the impedance relationship and with the surface perturbation winds (Fig. 3a), the perturbation horizontal motion (relative to the background motion) of the clouds in the wave ridges is clearly positive or in the direction of the wave motion. In the wave troughs, the perturbation motion of the clouds is clearly negative or opposite the direction of wave motion.

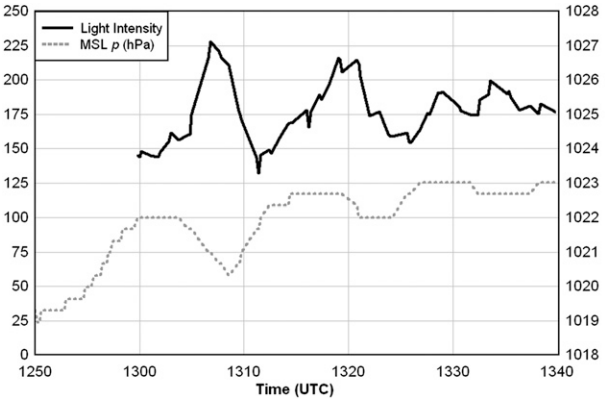

FIG. 6. Normalized light intensity (solid dark curve) and MSL pressure (dashed gray curve) at Tama Webcam site on 6 May 2007 (see text). The region in each frame of the time-lapse photography analyzed to determine light intensity is shown by the white line segment in Fig. 5a.

5. Conclusions

A strong undular bore was initiated when the cold pool associated with an MCS interacted with stable air in eastern Iowa on 6 May 2007. The bore and gravity waves were able to propagate because of a wave duct in place. The IEM Webcam at Tama, Iowa, was oriented so that its viewing angle was parallel to the bore and the waves and provided a time lapse that is one of the best photographic visualizations of gravity waves in the atmosphere ever captured. Consistent in time with surface pressure and wind observations, the cloud base became concave, and the sky became darker because of lift and condensation in the wave ridges. The cloud base was convex, and the sky became lighter because of subsidence and drying in the wave troughs. The wind perturbations and associated cloud motions, correlated with the pressure perturbations, may also be seen in the full time lapse.

Acknowledgments. Funding for this research is provided by grants from the National Oceanic and Atmospheric Administration (NA09OAR4600204) and from the NOAA Climate Prediction Program for the Americas (NA08OAR4310578).

REFERENCES

Christie, D. R., 1989: Long nonlinear waves in the lower atmosphere. *J. Atmos. Sci.,* **46,** 1462–1491.

——, K. J. Muirhead, and A. L. Hales, 1978: On solitary waves in the atmosphere. *J. Atmos. Sci.,* **35,** 805–825.

Clarke, R. H., R. K. Smith, and D. G. Reid, 1981: The morning glory of the Gulf of Carpentaria: An atmospheric undular bore. *Mon. Wea. Rev.,* **109,** 1726–1750.

Coleman, T. A., K. R. Knupp, and J. T. Tarvin, 2009: Review and case study of sounds associated with the lightning electromagnetic pulse. *Mon. Wea. Rev.,* **137,** 3129–3136.

Crook, N. A., 1986: The effect of ambient stratification and moisture on the motion of atmospheric undular bores. *J. Atmos. Sci.,* **43,** 171–181.

Glynn, E. F., cited 2003: Pixel profile lab report, EFG's Computer Lab. [Available online at http://www.efg2.com/Lab/ImageProcessing/PixelProfile.htm.]

Gossard, E. E., and W. H. Hooke, 1975: *Waves in the Atmosphere*. Vol. 2, *Developments in the Atmospheric Sciences,* Elsevier, 456 pp.

Hartung, D. C., J. A. Otkin, J. E. Martin, and D. D. Turner, 2010: The life cycle of an undular bore and its interaction with a shallow, intense cold front. *Mon. Wea. Rev.,* **138,** 886–908.

Knupp, K. R., 2006: Observational analysis of a gust front to bore to solitary wave transition within an evolving nocturnal boundary layer. *J. Atmos. Sci.,* **63,** 2016–2035.

Koch, S. E., and C. O'Handley, 1997: Operational forecasting and detection of mesoscale gravity waves. *Wea. Forecasting,* **12,** 253–281.

——, W. Feltz, F. Fabry, M. Pagowski, B. Geerts, K. M. Bedka, D. O. Miller, and J. W. Wilson, 2008: Turbulent mixing processes in atmospheric bores and solitary waves deduced from profiling systems and numerical simulation. *Mon. Wea. Rev.,* **136,** 1373–1400.

Lindzen, R. S., and K.-K. Tung, 1976: Banded convective activity and ducted gravity waves. *Mon. Wea. Rev.,* **104,** 1602–1617.

Nappo, C. J., 2002: *An Introduction to Atmospheric Gravity Waves*. Academic Press, 276 pp.

Rottman, J. W., and J. E. Simpson, 1989: The formation of internal bores in the atmosphere: A laboratory model. *Quart. J. Roy. Meteor. Soc.,* **115,** 941–963.

Scorer, R. S., 1949: Theory of waves in the lee of mountains. *Quart. J. Roy. Meteor. Soc.,* **75,** 41–56.

Simpson, J. E., 1997: *Gravity Currents: In the Environment and the Laboratory*. 2nd ed. Cambridge University Press, 244 pp.

Wakimoto, R. M., and D. E. Kingsmill, 1995: Structure of an atmospheric undular bore generated from colliding boundaries during CaPE. *Mon. Wea. Rev.,* **123,** 1374–1393.